

ANALYSIS FOR CONTACT ANGLE HYSTERESIS ON ROUGH SURFACES BY A PHASE-FIELD MODEL WITH A RELAXED BOUNDARY CONDITION*

XIANMIN XU[†], YINYU ZHAO[‡], AND XIAOPING WANG[§]

Abstract. In this paper, we study the contact angle hysteresis on a slowly moving rough boundary using a phase-field model with a relaxed boundary condition. In particular, we want to model the recent experimental observation in [D. Guan et al., *Phys. Rev. Lett.*, 116 (2016), 066102]. The speed of the moving boundary is slow enough so that the fluid flow effect is negligible. From asymptotic analysis, we derive an ordinary differential system for the dynamics of the apparent contact angle and the contact point. The system enables us to understand the contact angle hysteresis in the experiment, including the asymmetric dependence of the advancing and receding contact angles on the boundary velocity.

Key words. contact angle hysteresis, phase field equation, asymptotic analysis

AMS subject classifications. 41A60, 49Q05, 76T10

DOI. 10.1137/18M1182115

1. Introduction. Contact angle hysteresis is an interesting phenomenon in wetting problems [10, 11, 4]. When a liquid is moving on a solid surface, the advancing angle is usually different from the receding angle, as shown in Figure 1.1. This is called contact angle hysteresis (CAH). CAH is an unsolved problem in fluid dynamics [14, 27, 25, 31]. In general, CAH is believed to be mainly induced by the roughness or chemical inhomogeneity of the solid surface. Hysteresis is observed even on extremely smooth surfaces with nanodefects [17]. However, the quantitative understanding of the phenomena is still lacking. Recent experiments show that the advancing and receding contact angles may change with the wall velocity. This change of the contact angles may be asymmetric. It is observed that the receding contact angle is more sensitive to the change of the velocity than the advancing contact angle [18]. As far as we know, there is no clear theoretical analysis for such a phenomenon.

The CAH problem has been studied extensively [4]. There are plenty of experiments on various properties of CAH and also on its many applications in biology and technology [24, 30, 25, 41, 18]. Theoretical analysis of the problem is quite difficult. Most studies concentrate on the quasi-static process of CAH [16, 35]. For example, Joanny and de Gennes considered a smooth surface with very dilute defects so that the analysis for pinning the contact line by one defect can be applied [19].

From the mathematical point of view, theoretical study of CAH is also very challenging due to its multiscale feature [3]. The microscopic roughness or inhomogeneity

*Received by the editors April 19, 2018; accepted for publication (in revised form) September 4, 2019; published electronically December 12, 2019.

<https://doi.org/10.1137/18M1182115>

Funding: This work was partially supported by Chinese NSFC project 11971469, NSFC grant 91630208, and Hong Kong RGC-GRF 16324416.

[†]Corresponding author. LSEC, NCMIS, Academy of Mathematics and Systems Science, Chinese Academy of Sciences, Beijing 100190, China, and School of Mathematical Sciences, University of Chinese Academy of Sciences, Beijing 100049, China (xmxu@lsec.cc.ac.cn).

[‡]LSEC, ICMSEC, Academy of Mathematics and Systems Science, Chinese Academy of Sciences, Beijing 100190, China (zhaoyinyu@lsec.cc.ac.cn).

[§]Department of Mathematics, The Hong Kong University of Science and Technology, Clear Water Bay, Kowloon, Hong Kong, China (mawang@ust.hk).

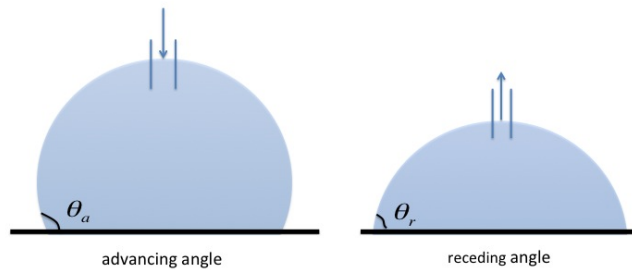


FIG. 1.1. *Contact angle hysteresis: the advancing angle is larger than the receding angle.*

of the solid surface may have a significant effect on the macroscopic properties of the contact angle. Because of the complexity of the problem, mathematical analysis of CAH mainly focuses on a simplified problem without flow effect. Then the problem will be modeled by minimizing the total surface energy in a liquid-vapor-solid system. The existence of many local minimizers of the energy minimization problem has been analyzed in [21, 5], and this can be used to understand CAH. In [1, 12, 32], some effective models are derived assuming an energy barrier when minimizing the energy. In [39], we did analysis for a quasi-static process of CAH for a two dimensional problem with chemically inhomogeneous surfaces. The analysis can be generalized to the three dimensional case by using a modified Wenzel and Cassie equation [40, 36]. In [34], we study a phase-field model with a relaxed boundary condition on chemically patterned surfaces.

In this paper, we aim to use the phase-field model to explain the asymmetric dependence of the advancing and receding contact angles on the wall velocity. We first generalize the analysis in [34] to a more general situation where the solid surface could be both geometrically rough and chemically inhomogeneous. We consider a Cahn–Hilliard equation with a relaxed boundary condition. Different from that in [34], we assume the solid boundary is moving with some given velocity. We derive the sharp-interface limit of the phase-field equation by asymptotic analysis. The dynamics for the contact point and the apparent contact angle (described by an ordinary differential system) are derived from the sharp-interface limit. The system can be reduced to the one in [34] when the geometrical roughness does not appear. By solving the ordinary differential system numerically, we observe the clear CAH behavior for various rough surfaces. Interestingly, the system can give quite similar phenomena of asymmetric dependence of CAH on wall velocity to that in experiments [18]. This indicates that our analysis captures some essential features of CAH. The analysis can also be generalized to the three dimensional case for problems with simple geometry.

The structure of the paper is as follows. In section 2, we introduce the phase-field model for the wetting problem. In section 3, asymptotic analysis is given to derive the sharp-interface limit of the phase-field equation. An ordinary differential system for the apparent contact angle and the contact points is derived in section 4. The generalization of the analysis to a three dimensional problem is given in section 5. Some numerical examples are illustrated in section 6. Conclusions and discussions are given in the last section.

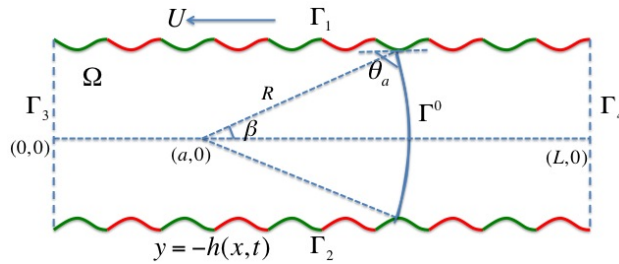


FIG. 2.1. A free interface in a channel with a periodically rough and inhomogeneous surface.

2. A phase field model for wetting problems. We consider a two-phase flow in a channel with geometrically rough boundary, as shown in Figure 2.1. The upper and lower boundaries are given by $y = \pm(h_0 + \delta H(\frac{x}{\delta}))$. Here $H(\cdot)$ is a periodic and differentiable function. Here $\delta \ll h_0$ is a small positive number. We assume that the boundary might also be chemically inhomogeneous in the sense that Young's angle θ_Y , the static contact angle of a liquid on a flat surface, is not a constant on the boundary. For simplicity, we assume $\theta_Y(x)$ is also a periodic function with period δ . Suppose the average horizontal velocity of the fluid is U . For convenience, we choose a frame moving with velocity U , and consider the problem in a domain $\Omega(t)$, whose boundaries moves with a velocity $-U$ horizontally. The domain $\Omega(t)$ is given by

$$(2.1) \quad \Omega(t) = \{(x, y) | 0 < x < L, -h(x, t) < y < h(x, t)\},$$

with $h(x, t) = h_0 + \delta H((x + Ut)/\delta)$. We assume L/ε is an integer so that the volume of $\Omega(t)$ does not change with time. As in [7], we assume

$$(2.2) \quad \max_x \{\sqrt{1 + (\partial_x h)^2} |\cos \theta_Y|\} < 1.$$

The condition implies that the roughness of the solid surface cannot be too strong. This is to avoid the existence of a Cassie–Baxter state where air is trapped under the liquid on the rough surface [6].

On a rough or chemically patterned surface, the interface will oscillate due to the stick-slip behaviors of the contact points [33]. The problem is quite complicated due to the existence of the moving contact line and the microscopic roughness of the boundary. In general, the moving contact line problem can be modeled by a coupled Navier–Stokes–Cahn–Hilliard system with a generalized Navier slip boundary condition [26]. When the fluid velocity is small, one can ignore the fluid effect and use a Cahn–Hilliard equation with a relaxed boundary condition to model the evolution of the contact angle [8]. The phase-field equation is a simplified model to describe the wetting phenomena qualitatively, and it may be a good approximation when the fluid is very viscous so that the velocity is small.

To study the evolution of the contact angle, we consider the following Cahn–Hilliard equation:

$$(2.3) \quad \begin{cases} \varepsilon \phi_t = \Delta \mu, \\ \mu = -\varepsilon \Delta \phi + \frac{F'(\phi)}{\varepsilon}, \end{cases}$$

with an initial condition $\phi(x, 0) = \phi_0(x)$. Here ϕ is the phase-field function, μ is the chemical potential, and $F(\phi) = \frac{(1-\phi^2)^2}{4}$ is the free energy density. The parameter $\varepsilon \ll \delta$ measures the interface thickness.

The boundary conditions on the upper boundary $\Gamma_1 := \{(x, y) | y = h(x, t), 0 < x < L\}$ and the lower $\Gamma_2 := \{(x, y) | y = -h(x, t), 0 < x < L\}$ are given by

$$(2.4) \quad \partial_n \mu = 0, \quad \varepsilon(\phi_t + u_{w,\tau} \partial_\tau \phi) = -\alpha(\varepsilon \partial_n \phi + \gamma'(x, t, \phi)).$$

Here the normal derivative $\partial_n = \mathbf{n} \cdot \nabla$ and \mathbf{n} is the unit exterior normal to the boundary of Ω , τ is the unit tangential direction of the boundary pointing right, $u_{w,\tau} = (-U, 0) \cdot \tau$ is the tangential velocity of the wall, and α is a relaxation parameter. The surface energy $\gamma(x, t, \phi) = \frac{\gamma_{SV} - \gamma_{SL}}{2} - \frac{\gamma_{SV} - \gamma_{SL}}{4} (3\phi - \phi^3)$. By Young's equation $\gamma_{SV} - \gamma_{SL} = \sigma \cos \theta_Y$ with Young's angle $\theta_Y(x + Ut)$, it can be simplified as

$$\gamma(x, t, \phi) = \frac{\gamma_{SV} - \gamma_{SL}}{2} - \frac{\sigma \cos \theta_Y(x + Ut)}{4} (3\phi - \phi^3).$$

Here $\sigma = \frac{2\sqrt{2}}{3}$ is the (dimensionless) liquid-vapor surface tension [22]. In addition, we use the notation $\gamma'(x, t, \phi) = \frac{\partial \gamma}{\partial \phi}$.

The second equation of (2.4) gives a dynamic boundary condition for the Cahn–Hilliard equation. If we ignore the term with $u_{w,\tau}$, the equation implies that the contact angle relaxes to the equilibrium Young's angle gradually [26]. The relaxation rate is proportional to an unbalanced Young's force $\varepsilon \partial_n \phi + \gamma'(x, t, \phi)$ with α being a phenomenological parameter. When α goes to infinity, the boundary condition will converge to a standard boundary condition for the Cahn–Hilliard equation; that is, the contact angle is equal to Young's angle. In this paper, we choose α as a fixed constant. Due to the motion of the solid wall, there is a convective term $u_{w,\tau} \partial_\tau \phi$ in the boundary condition. Since there exist many local equilibrium states in the system, even a small velocity can change the apparent contact angle dramatically.

The conditions on the boundaries $\Gamma_3 = \{(0, y) | -h(0, t) < y < h(0, t)\}$ and $\Gamma_4 = \{(L, y) | -h(L, t) < y < h(L, t)\}$ are given by

$$(2.5) \quad \partial_n \mu = 0, \quad \phi = 1 \quad \text{on } \Gamma_3,$$

$$(2.6) \quad \partial_n \mu = 0, \quad \phi = -1 \quad \text{on } \Gamma_4.$$

Here we assume $\phi = 1$ in the liquid domain and $\phi = -1$ in the vapor domain.

3. Sharp-interface limit of the phase-field model. We study the sharp-interface limit of the system (2.3)–(2.6) by the asymptotic matching method. In this section, we will use the notation $\mathbf{x} = (x, y)$ to represent the coordinate of a point in Ω .

3.1. The bulk equation. This asymmetric analysis for the bulk equation follows the standard approach for a phase-field equation [23].

Outer expansions. We first consider the asymptotic expansion of (2.3) far from the two-phase interface $\Gamma^\varepsilon(t)$. Suppose the leading order approximation of $\Gamma^\varepsilon(t)$ is $\Gamma^0(t)$. In the following, we write Ω instead of $\Omega(t)$ for simplicity. The domain Ω is divided by Γ^0 into two parts Ω^+ (the left part of Ω) and Ω^- (the right part of Ω). Suppose

$$\begin{aligned} \phi^\pm &= \phi_0^\pm + \varepsilon \phi_1^\pm + \cdots && \text{in } \Omega^\pm, \\ \mu^\pm &= \varepsilon^{-1} \mu_{-1}^\pm + \mu_0^\pm + \varepsilon \mu_1^\pm + \cdots && \text{in } \Omega^\pm. \end{aligned}$$

Here we let ϕ_0^+ be positive and ϕ_0^- negative. Substitute the above expansions into (2.3). The leading order is given by

$$(3.1) \quad O(\varepsilon^{-1}) : \quad \Delta \mu_{-1}^\pm = 0, \quad \mu_{-1}^\pm = F'(\phi_0^\pm) = (\phi_0^\pm)^3 - \phi_0^\pm,$$

and the next order is

$$(3.2) \quad O(1) : \quad \Delta\mu_0^\pm = 0, \quad \mu_0^\pm = (3(\phi_0^\pm)^2 - 1)\phi_1^\pm.$$

Substituting the expansions into the boundary conditions (2.4)–(2.6), we obtain

$$(3.3) \quad \partial_n\mu_{-1}^\pm = 0, \quad \partial_n\mu_0^\pm = 0 \quad \text{on } \partial\Omega^\pm,$$

$$(3.4) \quad \phi_0^+ = 1 \quad \text{on } \Gamma_3,$$

$$(3.5) \quad \phi_0^- = -1 \quad \text{on } \Gamma_4,$$

$$(3.6) \quad \gamma'(\phi_0^\pm) = 0 \quad \text{on } \partial\Omega^\pm \cap (\Gamma_1 \cup \Gamma_2).$$

Inner expansions. To analyze the sharp-interface limit of the Cahn–Hilliard equation, we need to consider the inner expansions near the interface Γ^0 . For that purpose, we denote $d(\mathbf{x})$ the signed distance function to Γ^0 and let $d(\mathbf{x}) < 0$ in Ω^- and $d(\mathbf{x}) > 0$ in Ω^+ . Then the unit normal of Γ^0 and the signed curvature κ of the interface are given by

$$\mathbf{n} = \nabla d, \quad \kappa = \Delta d.$$

It is easy to see that \mathbf{n} is the unit normal pointing into Ω^+ and $\kappa(\mathbf{x})$ is positive when Ω^- is convex near \mathbf{x} . We introduce a stretched variable near the interface Γ^0 ,

$$\xi = \frac{d(\mathbf{x})}{\varepsilon}.$$

Assume that ϕ and μ can be written in variables (\mathbf{x}, ξ, t) with expansions:

$$(3.7) \quad \phi = \tilde{\phi}_0(\mathbf{x}, \xi, t) + \varepsilon\tilde{\phi}_1(\mathbf{x}, \xi, t) + \dots,$$

$$(3.8) \quad \mu = \varepsilon^{-1}\tilde{\mu}_{-1}(\mathbf{x}, \xi, t) + \tilde{\mu}_0(\mathbf{x}, \xi, t) + \dots.$$

In the new coordinates, the derivatives can be rewritten as

$$\begin{aligned} \nabla &= \nabla_{\mathbf{x}} + \varepsilon^{-1}\mathbf{n}\partial_\xi, \\ \Delta &= \varepsilon^{-2}\partial_{\xi\xi} + \varepsilon^{-1}\kappa\partial_\xi + \Delta_{\mathbf{x}} + 2\mathbf{n} \cdot \nabla_{\mathbf{x}}\partial_\xi. \end{aligned}$$

We substitute the expansions (3.7)–(3.8) into (2.3) and use the above expressions for derivatives. To leading order, we have

$$(3.9) \quad \partial_{\xi\xi}\tilde{\mu}_{-1} = 0, \quad \tilde{\mu}_{-1} = -\partial_{\xi\xi}\tilde{\phi}_0 + F'(\tilde{\phi}_0),$$

and the next order is

$$(3.10) \quad \partial_{\xi\xi}\tilde{\mu}_0 = 0, \quad \tilde{\mu}_0 = -\partial_{\xi\xi}\tilde{\phi}_1 + \kappa\partial_\xi\tilde{\phi}_0 + 2(\mathbf{n} \cdot \nabla_{\mathbf{x}})\partial_\xi\tilde{\phi}_0 + F''(\tilde{\phi}_0)\tilde{\phi}_1.$$

We also have the next order expansion for $\tilde{\mu}_1$:

$$\partial_{\xi\xi}\tilde{\mu}_1 = 0.$$

By the first equation of (3.9), we have

$$\tilde{\mu}_{-1} = c_0\xi + c_1.$$

Using the matching condition for $\lim_{\xi \rightarrow \pm\infty} \tilde{\mu}_{-1} = \mu_{-1}^\pm$ and the boundedness of μ_{-1}^\pm , we obtain $c_0 = 0$ and

$$(3.11) \quad \mu_{-1}^\pm = c_1 \quad \text{on } \Gamma^0.$$

That means μ_{-1}^{\pm} is continuous across Γ^0 . Similarly, by the first equation of (3.10) and the matching condition of $\tilde{\mu}_0$, we know that $\tilde{\mu}_0$ is independent of ξ and μ_0^{\pm} is continuous across Γ^0 . In addition, by the matching condition

$$\lim_{\xi \rightarrow \pm\infty} \partial_{\xi} \tilde{\mu}_0 = \lim_{d(\mathbf{x}) \rightarrow \pm 0} \mathbf{n} \cdot \nabla_{\mathbf{x}} \mu_{-1}(\mathbf{x}),$$

we have $\mathbf{n} \cdot \nabla \mu_{-1} = 0$ on Γ^0 . Combining with (3.1), where $\Delta \mu_{-1}^{\pm} = 0$, we thus have that μ_{-1}^{\pm} are both constant functions such that

$$\mu_{-1}^{\pm} = c_1 \quad \text{in } \Omega^{\pm}.$$

This implies that μ_{-1} is constant in the whole domain Ω . Similar arguments lead to the fact that μ_0 is a constant in Ω .

Noticing that $\mu_{-1}^{\pm} = (\phi_0^{\pm})^3 - \phi_0^{\pm}$ and observing the boundary condition (3.4)–(3.5) on Γ_3 and Γ_4 , we have

$$\mu_{-1}^{\pm} = c_1 = 0 \quad \text{in } \Omega^{\pm}$$

and

$$\phi_0^{\pm}(\mathbf{x}) = \pm 1, \quad \mathbf{x} \in \Omega^{\pm}(t).$$

By the formula for $\tilde{\mu}_{-1}$ in (3.9), we have

$$(3.12) \quad -\partial_{\xi\xi} \tilde{\phi}_0 + F'(\tilde{\phi}_0) = 0.$$

Using the matching condition for $\tilde{\phi}_0$ that $\lim_{\xi \rightarrow \pm\infty} \tilde{\phi}_0 = \phi_0^{\pm} = \pm 1$, we know that the above equation has a unique solution $\tilde{\phi}_0 = \Phi(\xi) := \tanh(\frac{\xi}{\sqrt{2}})$. Here we use the fact that $F'(\tilde{\phi}_0) = \tilde{\phi}_0^3 - \tilde{\phi}_0$.

By the formula for $\tilde{\mu}_0$ and the fact that $\tilde{\mu}_0 = \mu_0$ is a constant, we have

$$\mu_0 = -\partial_{\xi\xi} \tilde{\phi}_0 + \kappa \partial_{\xi} \tilde{\phi}_0 + F''(\tilde{\phi}_0) \tilde{\phi}_0.$$

Multiply the above equation by $\partial_{\xi} \tilde{\phi}_0$: noticing also that $\tilde{\phi}_0$ satisfies (3.12), we obtain

$$(3.13) \quad 2\mu_0 = \kappa \int_{-\infty}^{+\infty} (\partial_{\xi} \tilde{\phi}_0)^2 d\xi = \kappa\sigma,$$

with $\sigma = \int_{-\infty}^{+\infty} (\partial_{\xi} \tilde{\phi}_0)^2 d\xi = \frac{2\sqrt{2}}{3}$. This implies that κ is a constant (since μ_0 is constant). In other words, the interface Γ_0 has constant curvature at any time. We would like to remark that the leading order equation (3.13) is different from that of the standard Cahn–Hilliard equation [23, 8]. This is because we choose a time scaling which leads to a very fast evolution of the Cahn–Hilliard equation to its equilibrium state. In this time scale, we only observe the evolution of an interface with constant curvature.

We will use this fact to do asymptotic analysis near the contact point in the following subsection.

3.2. Asymptotic analysis near the contact point. From the analysis above, we see that the curvature of Γ^0 is a constant changing with time. By symmetry of the channel with respect to the central line $y = 0$, we can assume that the limiting interface Γ^0 is a circle centered at $(a(t), 0)$ with radius $R(t)$ (as shown in Figure 2.1):

$$\Gamma^0(t) := \{(a(t), 0) + R(t)(\cos \vartheta, \sin \vartheta); |\vartheta| \leq \beta(t)\}.$$

Suppose the zero level set of ϕ_ε is given by

$$\Gamma^\varepsilon(t) := \{(a(t), 0) + R^\varepsilon(\vartheta, t)(\cos \vartheta, \sin \vartheta); |\vartheta| \leq \beta^\varepsilon(t)\}.$$

We can assume the expansion

$$R^\varepsilon(\vartheta, t) = R(t) + \varepsilon R_1(\vartheta, t) + \varepsilon^2 R_2(\vartheta, t) + \cdots.$$

Near the contact point on Γ_1 , we consider the stretched variables

$$\xi = \frac{R(t) - r}{\varepsilon}, \quad \eta = \frac{d_\Gamma(\mathbf{x})}{\varepsilon},$$

with $\mathbf{x} = (x, y)$ and $r = \sqrt{(x - a(t))^2 + y^2}$. Here d_Γ is the signed distance function to the upper boundary Γ_1 of Ω_ε , and $d_\Gamma(x, y) < 0$ for $y < h(x, t)$. In addition, we have $\vartheta = \arctan \frac{y}{x - a(t)}$.

We do analysis only near the contact point on Γ_1 . The contact point on Γ_2 can be analyzed similarly or by symmetry of the problem with respect to the plane $z = 0$. Denote $\phi(\mathbf{x}, t) = \hat{\phi}(\xi, \eta, t)$, $\mu(\mathbf{x}, t) = \hat{\mu}(\xi, \eta, t)$, and let \mathbf{n}_Γ be the outer normal of Γ_1 and \mathbf{n}_ϑ be the normal of Γ^0 pointing into Ω^+ . Here we do not use \mathbf{n}_{Γ_1} or \mathbf{n}_{ϑ_1} to make the notations simpler. It is easy to see that

$$\mathbf{n}_\Gamma = \nabla d_\Gamma \quad \text{and} \quad \mathbf{n}_\vartheta = -(\cos \vartheta, \sin \vartheta)^T.$$

By these notations, we easily have

$$\begin{aligned} \nabla \phi &= \varepsilon^{-1} \partial_\eta \hat{\phi} \mathbf{n}_\Gamma + \varepsilon^{-1} \partial_\xi \hat{\phi} \mathbf{n}_\vartheta, \\ \Delta \phi &= \varepsilon^{-2} \partial_{\eta\eta} \hat{\phi} + 2\varepsilon^{-2} \mathbf{n}_\Gamma \cdot \mathbf{n}_\vartheta \partial_{\eta\xi} \hat{\phi} + \varepsilon^{-2} \partial_{\xi\xi} \hat{\phi}, \\ \phi_t &= \varepsilon^{-1} (\dot{R} + \dot{a} \cos \vartheta) \partial_\xi \hat{\phi} + \partial_t \hat{\phi}. \end{aligned}$$

Here $\dot{R} = \frac{dR(t)}{dt}$ and \dot{a} is similarly defined. Similar equations hold for $\hat{\mu}$. Assume $\hat{\phi}$ has the following expansion:

$$\begin{aligned} \hat{\phi} &= \hat{\phi}^0(\xi, \eta, t) + \varepsilon \hat{\phi}^1(\xi, \eta, t) + \cdots, \\ \hat{\mu} &= \varepsilon^{-1} \hat{\mu}^{-1}(\xi, \eta, t) + \hat{\mu}^0(\xi, \eta, t) + \cdots. \end{aligned}$$

Substitute the expansions to (2.3) and the boundary condition (2.4). The leading order of the expansion gives

$$(3.14) \quad \begin{cases} \hat{\mu}_{\eta\eta}^{-1} + 2\mathbf{n}_\Gamma \cdot \mathbf{n}_\vartheta \hat{\mu}_{\eta\xi}^{-1} + \hat{\mu}_{\xi\xi}^{-1} = 0 & \text{when } \eta > 0, \\ \hat{\phi}_{\eta\eta}^0 + 2\mathbf{n}_\Gamma \cdot \mathbf{n}_\vartheta \hat{\phi}_{\eta\xi}^0 + \hat{\phi}_{\xi\xi}^0 - F'(\hat{\phi}^0) = \hat{\mu}^{-1} & \text{when } \eta > 0, \\ (\dot{R} + \dot{a} \cos \beta + u_{w,\tau} \cdot \mathbf{n}_\beta + \alpha \mathbf{n}_\Gamma \cdot \mathbf{n}_\beta) \hat{\phi}_\xi^0 = -\alpha(\hat{\phi}_\eta^0 + \gamma'(x_{ct}, t, \hat{\phi}^0)) & \text{when } \eta = 0. \end{cases}$$

Here x_{ct} is the x -coordinate of the contact point. We also have the matching condition that

$$(3.15) \quad \lim_{\eta \rightarrow +\infty} \hat{\mu}^{-1}(\xi, \eta, t) = \tilde{\mu}_{-1}(\xi, t), \quad \lim_{\eta \rightarrow +\infty} \hat{\phi}^0(\xi, \eta, t) = \tilde{\phi}_0(\xi, t).$$

It is easy to see that $\hat{\mu}^{-1}(\xi, \eta, t) = 0$ and $\hat{\phi}^0(\xi, \eta, t) = \Phi(\xi)$ are the solutions of the first two equations of (3.14) and the matching condition (3.15). Notice that

$$\gamma'(\hat{\phi}^0) = \frac{3\sigma}{4} ((\hat{\phi}^0)^2 - 1) \cos \theta_Y = -\cos \theta_Y \partial_\xi \Phi = -\cos \theta_Y \hat{\phi}_\xi^0.$$

Here we use θ_Y to represent $\theta_Y(x_{ct} + Ut)$ for simplicity of notation. Then the second equation of (3.14) gives

$$\dot{R} + \dot{a} \cos \beta = -\alpha(\mathbf{n}_\Gamma \cdot \mathbf{n}_\beta - \cos(\theta_Y)) - u_{w,\tau} \tau \cdot \mathbf{n}_\beta.$$

The equation gives a relation of $R(t)$, $a(t)$, and $\beta(t)$. We specify some notations in the above equation: $\tau = \frac{1}{\sqrt{1+(\partial_x h)^2}}(1, \partial_x h)^T$ and $\mathbf{n}_\Gamma = \frac{1}{\sqrt{1+(\partial_x h)^2}}(-\partial_x h, 1)^T$. Using the notation of the dynamic contact angle θ_d which satisfies $\cos \theta_d = \mathbf{n}_\Gamma \cdot \mathbf{n}_\beta$ and $\theta_d \in (0, \pi)$, the equation can be simplified as

$$(3.16) \quad \dot{R} + \dot{a} \cos \beta = \alpha[\cos \theta_Y(x_{ct} + Ut) - \cos \theta_d] + u_{w,\tau} \sin \theta_d.$$

By the bulk and boundary analysis, we see that the interface has constant mean curvature and the dynamic contact angle satisfies the boundary condition (3.16). Combining them together, the dynamics of the interface are completely determined.

4. Dynamics of the contact angle. By the above analysis, the leading order of the Cahn–Hilliard equation gives a circular interface which satisfies the condition (3.16) at the contact point. In the following, we will use the property to derive an equation for the contact point x_{ct} and the apparent contact angle θ_a :

$$(4.1) \quad \begin{cases} \dot{x}_{ct} = \frac{\alpha(\cos \theta_Y - \cos \theta_d)}{\sqrt{1+(\partial_x h(x_{ct}, t))^2} \sin \theta_d} - U \left(1 - \frac{\partial_x h(x_{ct}, t)}{1+(\partial_x h(x_{ct}, t))^2} \cot \theta_d \right), \\ \dot{\theta}_a = -\frac{\tilde{g}(\theta_a)}{h(x_{ct}, t)} \left[\left(\tilde{f}(\theta_a) \partial_x h(x_{ct}, t) + 1 \right) (\dot{x}_{ct} + U) - U \frac{h(0, t)}{h(x_{ct}, t)} \right]. \end{cases}$$

Here $\tilde{g}(\theta_a) = \frac{\cos^3 \theta_a}{\cos \theta_a + (\theta_a - \frac{\pi}{2}) \sin \theta_a}$ and $\tilde{f}(\theta_a) = \frac{(\theta_a - \frac{\pi}{2}) + \sin \theta_a \cos \theta_a}{\cos^2 \theta_a}$. They are two functions of the apparent angle and satisfy $1 \leq \tilde{g}(\theta_a) \leq 3$ and $-\frac{\pi}{2} \leq \tilde{f}(\theta_a) \leq \frac{\pi}{2}$. The apparent contact angle is the angle between the interface and the homogenized solid boundary, as shown in Figure 2.1. In general, the apparent contact angle θ_a is different from the dynamic contact angle θ_d on a rough surface. The relation between them is given in (4.16). Hence the system (4.1) is complete to describe the dynamics of x_{ct} and θ_a .

Before derivations of the system, we briefly discuss the physical meanings of the terms in (4.1). We start from the case when the solid surface is smooth and homogeneous. In this case, (4.1) is reduced to

$$(4.2) \quad \dot{x}_{ct} = \frac{\alpha(\cos \theta_Y - \cos \theta_d)}{\sin \theta_d} - U, \quad \dot{\theta}_d = -\frac{\tilde{g}(\theta_d)}{h_0} \left(\frac{\alpha(\cos \theta_Y - \cos \theta_d)}{\sin \theta_d} - U \right).$$

The term $(\cos \theta_Y - \cos \theta_d) / \sin \theta_d$ corresponds to the unbalanced Young's force [26, 38], which drives the dynamic contact angle to relax to its equilibrium value θ_Y . α is a relaxation rate parameter. The velocity term makes the dynamic contact angle differ from Young's angle when the wall moves. Since the contact angle and the contact point are related to each other under the volume conservation condition of the liquid, the motion of the contact point is also driven by these forces. The term \tilde{g} characterizes the difference of the relaxation processes of the contact angle and the contact point. The structure of the system (4.1) is the same as (4.2). The main difference is that the local geometry of the rough surface introduces some corrections in certain terms. All the corrections are related to $\partial_x h$ or $h(x_{ct}) - h(0)$ (noticing that $U - U \frac{h(0)}{h(x_{ct})} = U \frac{h(x_{ct}) - h(0)}{h(x_{ct})}$ in the second equation of (4.1)). That is because the local slope of the solid surface affects the equilibrium profile of the fluid interface and also makes the volume conservation constraints more complicated.

4.1. Derivation of (4.1). We first notice that the Cahn–Hilliard equation satisfies the following mass conservation property:

$$(4.3) \quad \frac{d}{dt} \int_{\Omega} \phi dx = 0.$$

This can be obtained by integration of the first equation of (2.3) and the use of the homogeneous Neumann boundary condition of μ . The leading order of (4.3) leads to

$$\frac{d}{dt} \int_{\Omega} \phi_0 dx = 0, \text{ or equivalently } (|\Omega^+| - |\Omega^-|) = \text{const.}$$

Noticing that $|\Omega^+| + |\Omega^-| = |\Omega| = \text{const}$, we have that the volumes of both Ω^+ and Ω^- are preserving. Denote A as the volume of Ω^+ . It is easy to compute that

$$(4.4) \quad A = R^2(\beta - \sin \beta \cos \beta) + 2 \int_0^{x_{ct}} h(x, t) dx,$$

where x_{ct} is the x -coordinate of the contact point. We also have the following geometric relation:

$$(4.5) \quad R \sin \beta = h(x_{ct}, t), \quad x_{ct} = a + R(t) \cos \beta.$$

We will use (3.16), (4.4), and (4.5) to derive the ODEs for β and x_{ct} .

By (4.4), using $\frac{dA}{dt} = 0$, we have

$$(4.6) \quad R\dot{R}(\beta - \sin \beta \cos \beta) + R^2\dot{\beta} \sin^2 \beta + h(x_{ct}, t)\dot{x}_{ct} + \int_0^{x_{ct}} \partial_t h(x, t) dx = 0.$$

The time derivative of (4.5) gives

$$(4.7) \quad \dot{R} \sin \beta + (R \cos \beta)\dot{\beta} = \partial_x h(x_{ct}, t)\dot{x}_{ct} + \partial_t h(x_{ct}, t),$$

$$(4.8) \quad \dot{a} + \dot{R} \cos \beta - (R \sin \beta)\dot{\beta} = \dot{x}_{ct}.$$

Multiply (4.7) by $\sin \beta$ and (4.8) by $\cos \theta$, and add them together; then we obtain

$$(4.9) \quad \dot{R} + \dot{a} \cos \beta = \dot{x}_{ct} [\cos \beta + \partial_x h(x_{ct}, t) \sin \beta] + \partial_t h(x_{ct}, t) \sin \beta.$$

Substituting (4.9) into (3.16) and simple computations lead to

$$(4.10) \quad \dot{x}_{ct} = \frac{\alpha(\cos \theta_Y(x_{ct} + Ut) - \cos \theta_d) + u_{w,\tau} \sin \theta_d - \partial_t h(x_{ct}, t) \sin \beta}{\cos \beta + \partial_x h(x_{ct}, t) \sin \beta}.$$

This is an ODE of the contact point x_{ct} , which depends on the unknown β . In the following, we will derive the equation of β . Using the first equation of (4.5), equation (4.6) is reduced to

$$\dot{R} h(x_{ct}, t) \frac{\beta - \sin \beta \cos \beta}{\sin \beta} + h^2(x_{ct}, t)\dot{\beta} + h(x_{ct}, t)\dot{x}_{ct} + \int_0^{x_{ct}} \partial_t h(x, t) dx = 0.$$

Combining with (4.7) and using the first equation of (4.5), we can eliminate \dot{R} and obtain by direct calculations that

$$(4.11) \quad \dot{\beta} = -g(\beta) \left[\frac{\sin^2 \beta + (\beta - \sin \beta \cos \beta) \partial_x h(x_{ct}, t)}{h(x_{ct}, t)} \dot{x}_{ct} + \frac{(\beta - \sin \beta \cos \beta) \partial_t h(x_{ct}, t)}{h(x_{ct}, t)} + \frac{\sin^2 \beta}{h^2(x_{ct}, t)} \int_0^{x_{ct}} \partial_t h(x, t) dx \right],$$

where $g(\beta) = \frac{\sin \beta}{\sin \beta - \beta \cos \beta}$. Equations (4.10) and (4.11) compose a complete system to describe the dynamics of the contact point and β , noticing the following formula on the dynamic contact angle:

$$(4.12) \quad \cos \theta_d = \mathbf{n}_\Gamma \cdot \mathbf{n}_\beta = \frac{\partial_x h(x_{ct}, t) \cos \beta - \sin \beta}{\sqrt{1 + (\partial_x h(x_{ct}, t))^2}},$$

$$(4.13) \quad \sin \theta_d = -\tau \cdot \mathbf{n}_\beta = \frac{\partial_x h(x_{ct}, t) \sin \beta + \cos \beta}{\sqrt{1 + (\partial_x h(x_{ct}, t))^2}}.$$

Assume the parameter δ is small in the formula of $h(x, t)$ and the rough boundary $y = h(x, t)$ approximates to an effective flat boundary $y = h_0$. Then the apparent contact angle will be $\theta_a = \beta + \frac{\pi}{2}$ (see Figure 2.1). Then (4.10) and (4.11) could be reduced to a system on θ_a and x_{ct} . Using the formula for u_w, τ , direct calculations give

$$(4.14) \quad \begin{cases} \dot{x}_{ct} = \frac{\alpha(\cos \theta_Y(x_{ct} + Ut) - \cos \theta_d)}{\sin \theta_a - \partial_x h(x_{ct}, t) \cos \theta_a} - \left[\frac{1}{1 + (\partial_x h(x_{ct}, t))^2} - \frac{\partial_x h(x_{ct}, t) \cos \theta_a}{\sin \theta_a - \partial_x h(x_{ct}, t) \cos \theta_a} \right] U, \\ \dot{\theta}_a = -\frac{\tilde{g}(\theta_a)}{h(x_{ct}, t)} \left[(\tilde{f}(\theta_a) \partial_x h(x_{ct}, t) + 1) \dot{x}_{ct} + (\tilde{f}(\theta_a) \partial_x h(x_{ct}, t) + \frac{1}{h(x_{ct}, t)} \int_0^{x_{ct}} H'(\frac{x+Ut}{\delta}) dx) U \right], \end{cases}$$

where we use the notations

$$\tilde{g}(\theta_a) = \frac{\cos^3 \theta_a}{\cos \theta_a + (\theta_a - \frac{\pi}{2}) \sin \theta_a}, \quad \tilde{f}(\theta_a) = \frac{\theta_a - \frac{\pi}{2} + \sin \theta_a \cos \theta_a}{\cos^2 \theta_a}.$$

Equation (4.14) can be further simplified. Using the fact that

$$\int_0^{x_{ct}} H' \left(\frac{x + Ut}{\delta} \right) dx = \delta \left(H \left(\frac{x_{ct} + Ut}{\delta} \right) - H \left(\frac{Ut}{\delta} \right) \right) = h(x_{ct}, t) - h(0, t),$$

the second equation of (4.14) is reduced to

$$(4.15) \quad \dot{\theta}_a = -\frac{\tilde{g}(\theta_a)}{h(x_{ct}, t)} \left[(\tilde{f}(\theta_a) \partial_x h(x_{ct}, t) + 1) (\dot{x}_{ct} + U) - U \frac{h(0, t)}{h(x_{ct}, t)} \right].$$

By (4.12)–(4.13), we have

$$(4.16) \quad \sin \theta_d = \frac{\sin \theta_a - \partial_x h(x_{ct}, t) \cos \theta_a}{\sqrt{1 + (\partial_x h(x_{ct}, t))^2}}, \quad \cos \theta_d = \frac{\partial_x h(x_{ct}, t) \sin \theta_a + \cos \theta_a}{\sqrt{1 + (\partial_x h(x_{ct}, t))^2}};$$

then the first equation of (4.14) can be simplified as

$$(4.17) \quad \dot{x}_{ct} = \frac{\alpha(\cos \theta_Y - \cos \theta_d)}{\sqrt{1 + (\partial_x h(x_{ct}, t))^2} \sin \theta_d} - U \left(1 - \frac{\partial_x h(x_{ct}, t)}{1 + (\partial_x h(x_{ct}, t))^2} \cotan \theta_d \right).$$

Combining them together, we obtain (4.1).

4.2. Discussions on the ODE system (4.1). First, it is easy to see that (4.1) is well-posed. Actually, since the right-hand-side terms of the equation are smooth functions, one can compute their derivatives with respect to θ_a and x_{ct} . The derivatives are bounded when the dynamic contact angle satisfies $c_0 < \theta_d < \pi - c_0$ for

some positive constant c_0 . This holds under the condition (2.2) and for sufficiently small U .

Second, when the boundary is flat so that $h \equiv h_0$, then $\theta_a = \theta_d$ and (4.1) is reduced to

$$(4.18) \quad \begin{cases} \dot{x}_{ct} = \frac{\alpha(\cos \theta_Y(x_{ct}+Ut) - \cos \theta_a)}{\sin \theta_a} - U, \\ \dot{\theta}_a = -\frac{\cos^3 \theta_a}{\cos \theta_a + (\theta_a - \frac{\pi}{2}) \sin \theta_a} \frac{\dot{x}_{ct}}{h_0}. \end{cases}$$

If we denote $\hat{x}_{ct} = x_{ct} + Ut$, the actual contact point on the boundary, the equation is reduced to

$$\begin{cases} \dot{\hat{x}}_{ct} = \frac{\alpha(\cos \theta_Y(\hat{x}_{ct}) - \cos \theta_a)}{\sin \theta_a}, \\ \dot{\theta}_a = -\frac{\cos^3 \theta_a}{\cos \theta_a + (\theta_a - \frac{\pi}{2}) \sin \theta_a} \frac{\dot{\hat{x}}_{ct} + U}{h_0}. \end{cases}$$

This is the same as the equation derived in [34]. There we did some analysis for the reduced model. We show that on a chemically patterned surface the ODE system behaves differently when the velocity U converges to zero from two sides. More precisely, we assume the solid surface is composed by two materials with different Young's angles θ_{Y1} and θ_{Y2} ($\theta_{Y1} > \theta_{Y2}$). Suppose the period δ is small. Then when $U \rightarrow 0^+$, the apparent contact angle will oscillate around θ_{Y1} , which corresponds to an advancing angle. When $U \rightarrow 0^-$, the contact angle will oscillate around θ_{Y2} , which corresponds to a receding angle. This is consistent with previous studies on quasi-static CAH [19, 39].

Third, we further assume the solid surface is homogeneous so that $\theta_Y(x) \equiv \theta_{Y0}$ for a constant θ_{Y0} . The ODE system (4.18) will have a steady state, which satisfies the equation

$$(4.19) \quad \frac{\alpha(\cos \theta_{Y0} - \cos \theta_a)}{\sin \theta_a} - U = 0.$$

This implies that the apparent contact angle θ_a is uniquely determined by θ_{Y0} and U . When U goes to zero, the angle will converge to θ_{Y0} . To leading order, we have

$$U \propto (\theta_a - \theta_{Y0}).$$

It gives a simplified relation between the apparent contact angle and the wall velocity U . The relation is different from the Cox–Voinov-type relations in the literature [9, 29] since we do not consider the viscous dissipations in our system.

5. Extension to the three dimensional case. The analysis in the above sections can be extended to a three dimensional case if the problem has simple geometry. As an example, we consider the two-phase flow in a three dimensional channel. We assume that the channel is axisymmetric with respect to the x -axis. In a cylindrical coordinate system (r, ψ, x) , the solid boundary is given by

$$r = h(x).$$

We assume h is a smooth function and periodic in x with period δ . We consider the Cahn–Hilliard equation (2.3) in the channel with a relaxed boundary condition on the solid boundary. Suppose the solution of the equation is also axisymmetric.

The asymptotic analysis in section 3.1 can be extended to this case in a straightforward way. To leading order, the two-phase interface has a constant mean curvature at every time t . Due to its axis symmetry, the interface is spherical. It intersects

with the solid boundary with a circular contact line $r = h(x_{ct})$, with x_{ct} being the x -coordinate of the contact line. Suppose the interface has a radius R centered at $(0, 0, a)$. Careful analysis near the contact line leads to a boundary condition

$$(5.1) \quad \dot{R} + \dot{a} \cos \beta = \alpha(\cos \theta_Y - \cos \theta_d) + u_{w,\tau} \sin \theta_d$$

which has the same form as (3.16). Here β has a definition similar to that in the two dimensional case.

Similar to that in section 4, we can also derive an ODE system for the apparent contact angle and the contact line. The system will be slightly different from that in two dimensions. Denote V as the volume of Ω^+ , the domain on the left side of the interface. We can compute the volume

$$V = \frac{\pi}{3} R^3 (2 - \cos \beta)(1 - \cos \beta)^2 + \pi \int_0^{x_{ct}} h^2(x) dx.$$

By $\frac{dV}{dt} = 0$, we have

$$(5.2) \quad R^2 \dot{R} (2 + \cos \beta)(1 - \cos \beta)^2 + R^3 \dot{\beta} \sin^3 \beta + h^2(x_{ct}, t) \dot{x}_{ct} + \int_0^{x_{ct}} \partial_t h^2(x_{ct}, t) dx = 0.$$

Replace (4.6) by (5.2), and do calculations similar to those in section 4.1. We can obtain an equation for β ,

$$(5.3) \quad \dot{\beta} = - \left[\frac{\dot{x}_{ct} (1 + \cos \beta)(3 - \cos^3 \beta)}{h(x_{ct}, t)} + \frac{\partial_t h(x_{ct}, t)}{h(x_{ct}, t)} (2 + \cos \beta) \sin^2 \beta + \frac{(1 + \cos \beta)^2}{h^3} \int_0^{x_{ct}} \partial_t h^2(x, t) dx \right].$$

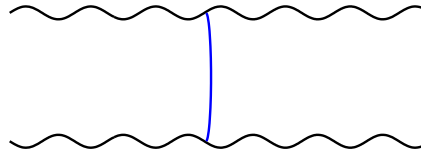
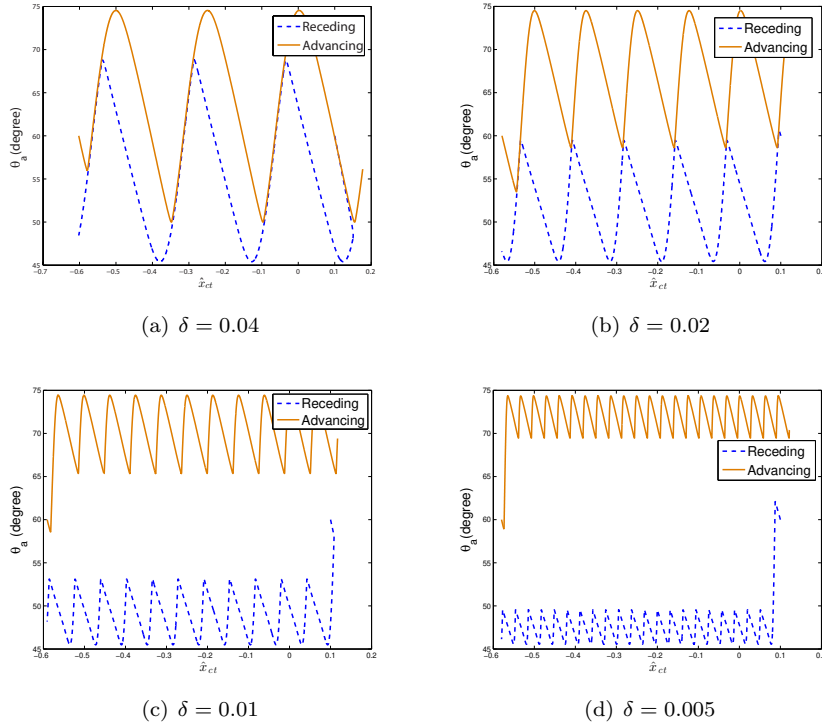
The equation is different from (4.11). In addition, we could derive an equation for x_{ct} , which is the same as (4.10).

In the above analysis, we assume that the three dimensional problem is axisymmetric. Therefore, the results are similar to those in the two dimensional case. In general, the analysis for a three dimensional problem will be more complicated. If the roughness of the solid surface is periodic, we may first do homogenization for the system to derive a reduced problem defined in a domain with a homogenized boundary [40, 36, 19]. Then similar analysis can be done for the reduced problem.

6. Numerical examples. In this section, we will give some numerical examples to show that the ODE system (4.14) can be used to understand the interesting CAH phenomena. In these examples, we set $\alpha = 1$.

Example 1. In the first example, we consider a smoothly oscillating boundary, as shown in Figure 6.1. The boundary is given by $h(x, t) = h_0 + \delta H((x + Ut)/\delta)$, and we set $h_0 = 0.8$, $H = \frac{\sin x}{4}$, and $U = \pm 0.01$. We did experiments for several choices of δ . We choose $\theta_Y = \frac{\pi}{3}$. We solve the ODE system (4.14) numerically. Some typical numerical results are given in Figure 6.2.

In every subplot, we draw two curves on the trajectories of the solution of the ODE system in phase plane. Here we show the apparent contact angle with respect to the actual position \hat{x}_{ct} of the contact point on the rough boundary. The lower curve corresponds to a negative velocity U , and the upper one corresponds to a positive U . When $U < 0$, the boundary moves to the right and we observe a receding contact angle. Similarly, when $U > 0$, we observe an advancing contact angle.

FIG. 6.1. *The channel with smooth oscillating boundaries.*FIG. 6.2. *The apparent contact angle θ_a and the x -coordinate of the contact point \hat{x}_{ct} in a channel with a different oscillating rough boundary.*

For the case where $\delta = 0.04$, the period of the oscillation of the boundary is relatively large. We could see that the two trajectories overlap and the intervals of the advancing angle and receding angle are almost the same. One can hardly observe the CAH. On the other hand, when δ becomes smaller, which means that the boundary is more oscillating, the CAH becomes more obvious.

When $\delta = 0.005$, we can see that the maximal advancing angle is about 74° and the minimal receding contact angle is about 46° even when the initial values of the contact angle are far from the two values, as shown by the left end of the red (solid) curve and the right end of the blue (dashed) curve. This is consistent with previous analysis and computations. By the modified Wenzel's equation [36], the maximal/minimal apparent contact angle of a liquid (in equilibrium) on an oscillating boundary is equal to $\theta_Y \pm \theta_g$, with θ_g being the largest angle of inclination of the boundary. In this example, the largest slope of the rough boundary is $1/4$ and so

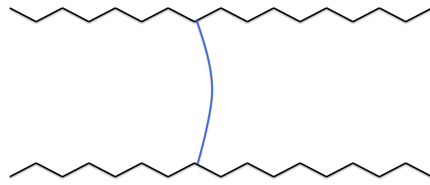


FIG. 6.3. The channel with serrated boundaries.

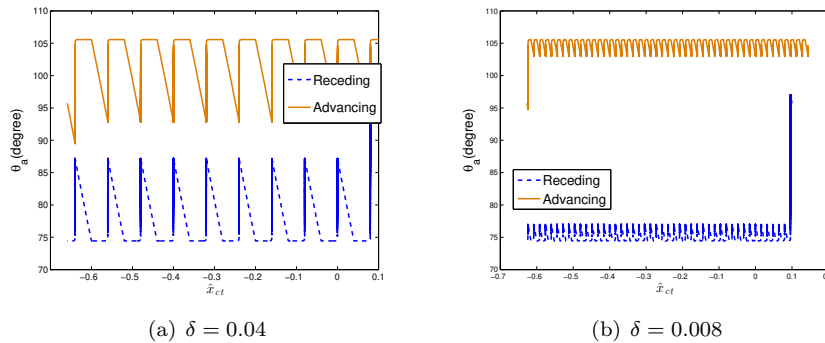


FIG. 6.4. CAH on a rough boundary with a serrated shape.

that $\theta_g = \arctan(1/4) \approx 14.04^\circ$. This means that with small velocity $U = 0.01$, the advancing angle and the receding angle approach, respectively, the maximal and minimal apparent contact angles in equilibrium.

Example 2. In the second example, we consider a tube with nonsmooth oscillating rough boundaries. For simplicity, we choose a serrated shape of the boundary, as shown Figure 6.3. We can define $h(x, t) = h_0 + \delta H((x + Ut)/\delta)$, with $H(x)$ being a periodic function with period 2:

$$H(x) = \begin{cases} kx, & 0 < x < 1, \\ -kx, & 1 < x < 2. \end{cases}$$

Here we let $k = \tan(\pi/12)$. We choose the static Young's angle to be $\theta_Y = \pi/2$ and $U = \pm 0.01$. Notice that the function $h(x, t)$ is not differentiable at some points. But we still can solve the ODE system (4.14) numerically by setting $H'(x)$ to be its left or right limit of H' at these points. The numerical results are similar to those in the previous example. We show only a few results in Figure 6.4 for the choices $\delta = 0.04$ and $\delta = 0.008$. We can see the obvious CAH phenomena. When $\delta = 0.04$, we can see clear stick-slip behavior from the trajectories. At some positions, the contact point is pinned while the contact angle changes. The slip occurs with dramatic changes of both the contact position and the contact angle. Furthermore, numerical results indicate that the stick-slip behavior occurs only on the discontinuous points of the boundary. For example, the contact point on the lower boundary is pinned only at the highest vertexes of the surface and slips at the lowest points. From the case $\delta = 0.008$, we see that the advancing angle is about $7\pi/12 = 105^\circ$ and the receding angle is $5\pi/12 = 75^\circ$, which can be described again by the modified Wenzel's equation, noticing that $\theta_Y = \pi/2$ and $\theta_g = \pi/12$ in this case.

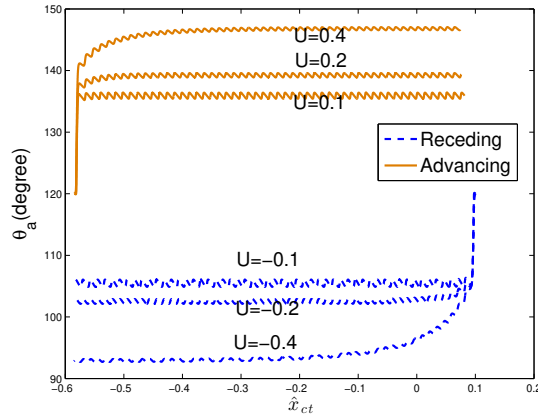


FIG. 6.5. Wall-velocity dependence of the CAH in Example 3 (with relatively small velocity).

Example 3. In the third example, we consider the effect of the velocity. Suppose the rough boundary is similar to that in Example 1. Here we choose $\delta = 0.002$ and $\theta_Y = 2\pi/3$. We solve the problem (4.14) with varying velocity U . The numerical results are shown in Figure 6.5. We see that with increasing velocity, the advancing angle becomes larger and the receding angle becomes smaller. The changes of the contact angle are almost symmetric, although the decreasing of the contact angle seems slightly faster. The decrease of the receding angle is about 10° (on average) when the velocity U changes from -0.2 to -0.4 , which is slightly larger than the increase (about 7°) of the advancing angle when the velocity changes from 0.2 to 0.4 .

Example 4. In the last example, we consider the wall-velocity dependence of the CAH on a chemically patterned surface. In this calculation, we consider a flat boundary $h = 0.5$ and assume $\theta_Y(x)$ is a periodic function with period 0.2 . In each period, $\theta_Y(x)$ is equal to $3\pi/4$ in a half of the period and $9\pi/10$ in the other half. We consider several choices of the velocity. The velocity is relatively larger than that in previous examples. The numerical results are shown the left subfigure of Figure 6.6. In this case, we can see the asymmetry of the wall-velocity dependence of the contact angles, which means that the changes of the advancing and receding contact angles are different with increasing velocity. This phenomenon occurs since the velocity is relatively large and the asymmetric choice of Young's angles is around $\frac{\pi}{2}$. If the Young's angles of the chemically patterned surface are symmetric with respect to $\frac{\pi}{2}$, the velocity dependence of the advancing and receding angles is also symmetric. In addition, if the velocity is small enough, the asymmetry of the velocity dependence is not obvious, as in the previous example.

Interestingly, the similar asymmetry of the wall-velocity dependence of the CAH has been observed in the experiments [18]; see the right subfigure in Figure 6.6. We can see that the numerical results looks similar to those in the physical experiments. This indicates that the ODE system captures some essential feature of CAH. We believe that the asymmetric dependence of the CAH on velocity is mainly caused by the asymmetric distribution of the chemical or geometrical inhomogeneity on the solid surface. On a homogeneous surface, there is no asymmetric velocity dependence of the contact angles. Finally, we would like to remark that the numerical results do not

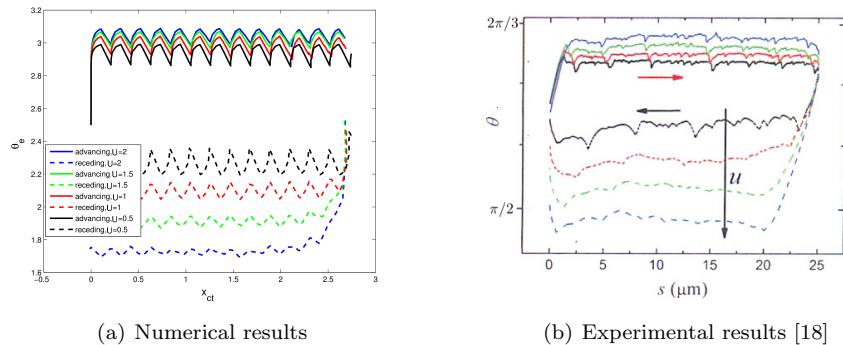


FIG. 6.6. *Nonsymmetric of wall-velocity dependence of CAH in Example 4 (with relatively large velocity).*

match the experiments quantitatively. There are many reasons for that. One obvious one is that the geometric setups are not the same. In our case, we simply consider a channel with a rough boundary. In the physical experiments, they considered a fibre pulling out and pushing into a liquid bath [18].

7. Conclusions. We study CAH by using a phase-field equation with a relaxed boundary condition on a moving rough surface. By asymptotic analysis, we derive a nonlinear ordinary differential system for the apparent contact angle and the contact point. The system can be used to understand some typical phenomena for CAH, including the asymmetry of the dependence of the advancing and receding contact angles on the velocity, which has been observed in experiments recently, i.e., the phenomena as shown in Example 3 in section 6. Some observations are obtained from our numerical examples. First, the advancing and receding contact angles can be characterized by the modified Wenzel or Cassie equations [36] when the velocity of the two-phase interface is small, as in quasi-static wetting problem. Second, the asymmetry of the velocity dependence of CAH is induced by the asymmetry of the chemical or geometric properties of the solid surface. It is more obvious for relatively larger velocities.

As far as we know, the analysis for the wall-velocity dependence of CAH is new. The phenomenon cannot be described by the previous quasi-static analysis for CAH as in [19, 39]. The main reason is that for quasi-static analysis, the relaxation dynamics of the contact angle to its equilibrium state are missing. The dynamics are described by the relaxed boundary condition in the phase-field model studied in the paper. In addition, the wall velocity cannot be included in the quasi-static models. The essential feature of the wall-velocity dependence can be captured very nicely in our model, although we do not consider the viscous effect of the fluid. Other contributions of the paper include the analysis for the sharp-interface limit for the phase-field model with a relaxed boundary condition on geometrically or chemically rough surfaces. The relaxed boundary condition is nontrivial in mathematics and has induced some interest recently [8, 20]. Finally, we derive a nonlinear ordinary differential system for the contact angle and the contact point, which is more complicated than that on the flat surface.

We remark that we do not consider the fluid effects in our study. The dissipation in the fluid might be important to quantify CAH, especially when the fluid velocity is

large. Although numerical simulations are possible as in [33, 28], theoretical analysis for that problem will be much more difficult. A recently developed strategy using the Onsager principle as an approximation tool might be useful for the analysis [37, 13].

Another important issue is to consider CAH on a more general and practical rough surface. The contact line can be pinned by the randomly distributed defects. The stochastic oscillation of the contact line may also be important for its motion on the rough surface. These will be considered in further work.

Mathematically, it is very interesting to prove rigorously the asymptotic analysis results. Due to the existence of the relaxed boundary condition, this is a nontrivial problem. Standard methods by a spectral estimate for the Cahn–Hilliard operator with standard boundary conditions [2] or by an analysis of the viscous solutions [15] cannot be used directly. This will be left for future study.

Acknowledgment. We thank the anonymous referees for their valuable comments and suggestions, which helped us to improve the manuscript greatly.

REFERENCES

- [1] G. ALBERTI AND A. DESIMONE, *Quasistatic evolution of sessile drops and contact angle hysteresis*, Arch. Ration. Mech. Anal., 202 (2011), pp. 295–348.
- [2] N. ALIKAKOS, P. BATES, AND X. CHEN, *Convergence of the Cahn–Hilliard equation to the Hele–Shaw model*, Arch. Rational Mech. Anal., 128 (1994), pp. 165–205.
- [3] A. L. BERTOZZI, *The mathematics of moving contact lines in thin liquid films*, Notices Amer. Math. Soc., 45 (1998), pp. 689–697.
- [4] D. BONN, J. EGGERS, J. INDEKEU, J. MEUNIER, AND E. ROLLEY, *Wetting and spreading*, Rev. Modern Phys., 81 (2009), pp. 739–805.
- [5] L. A. CAFFARELLI AND A. MELLET, *Capillary drops: Contact angle hysteresis and sticking drops*, Calc. Var. Partial Differential Equations, 29 (2007), pp. 141–160.
- [6] A. CASSIE AND S. BAXTER, *Wettability of porous surfaces*, Trans. Faraday Soc., 40 (1944), pp. 546–551.
- [7] X. CHEN, X.-P. WANG, AND X. XU, *Effective contact angle for rough boundary*, Phys. D, 242 (2013), pp. 54–64.
- [8] X. CHEN, X.-P. WANG, AND X. XU, *Analysis of the Cahn–Hilliard equation with relaxation boundary condition modelling contact angle*, Arch. Ration. Mech. Anal., 213 (2014), pp. 1–24.
- [9] R. COX, *The dynamics of the spreading of liquids on a solid surface, Part 1: Viscous flow*, J. Fluid Mech., 168 (1986), pp. 169–194.
- [10] P. G. DE GENNES, *Wetting: Statics and dynamics*, Rev. Modern Phys., 57 (1985), pp. 827–863.
- [11] P. G. DE GENNES, F. BROCHARD-WYART, AND D. QUERE, *Capillarity and Wetting Phenomena*, Springer, Berlin, 2003.
- [12] A. DESIMONE, N. GRUENEWALD, AND F. OTTO, *A new model for contact angle hysteresis*, Netw. Heterog. Media, 2 (2007), pp. 211–225.
- [13] Y. DI, X. XU, AND M. DOI, *Theoretical analysis for meniscus rise of a liquid contained between a flexible film and a solid wall*, Europhys. Lett., 113 (2016), 36001.
- [14] H. Y. ERBIL, *The debate on the dependence of apparent contact angles on drop contact area or three-phase contact line: A review*, Surf. Sci. Rep., 69 (2014), pp. 325–365.
- [15] L. C. EVANS, H. M. SONER, AND P. E. SOUGANIDIS, *Phase transitions and generalized motion by mean curvature*, Comm. Pure Appl. Math., 45 (1992), pp. 1097–1123.
- [16] L. GAO AND T. MCCARTHY, *Contact angle hysteresis explained*, Langmuir, 22 (2006), pp. 6234–6237.
- [17] A. GIACOMELLO, L. SCHIMMELE, AND S. DIETRICH, *Wetting hysteresis induced by nanodefects*, Proc. Natl. Acad. Sci. USA, 113 (2016), pp. E262–E271.
- [18] D. GUAN, Y. WANG, E. CHARLAIX, AND P. TONG, *Asymmetric and speed-dependent capillary force hysteresis and relaxation of a suddenly stopped moving contact line*, Phys. Rev. Lett., 116 (2016), 066102.
- [19] J. F. JOANNY AND P.-G. DE GENNES, *A model for contact angle hysteresis*, J. Chem. Phys., 81 (1984), pp. 552–562.
- [20] C. LIU AND H. WU, *An energetic variational approach for the Cahn–Hilliard equation with*

- dynamic boundary condition: Model derivation and mathematical analysis*, Arch. Ration. Mech. Anal., 23 (2019), pp. 167–247.
- [21] A. MELLET AND J. NOLEN, *Capillary drops on a rough surface*, Interfaces Free Bound., 14 (2012), pp. 167–184.
- [22] L. MODICA, *Gradient theory of phase transitions with boundary energy*, Ann. Inst. H. Poincaré Anal. Non Linéaire, 4 (1987), pp. 487–512.
- [23] R. PEGO, *Front migration in the nonlinear Cahn-Hilliard equation*, Proc. Roy. Soc. London Ser. A, 422 (1989), pp. 261–278.
- [24] C. PRIEST, R. SEDEV, AND J. RALSTON, *Asymmetric wetting hysteresis on chemical defects*, Phys. Rev. Lett., 99 (2007), 026103.
- [25] C. PRIEST, R. SEDEV, AND J. RALSTON, *A quantitative experimental study of wetting hysteresis on discrete and continuous chemical heterogeneities*, Colloid Polym. Sci., 291 (2013), pp. 271–277.
- [26] T. QIAN, X.-P. WANG, AND P. SHENG, *Molecular scale contact line hydrodynamics of immiscible flows*, Phys. Rev. E (3), 68 (2003), 016306.
- [27] R. RAJ, R. ENRIGHT, Y. ZHU, S. ADERA, AND E. N. WANG, *Unified model for contact angle hysteresis on heterogeneous and superhydrophobic surfaces*, Langmuir, 28 (2012), pp. 15777–15788.
- [28] W. REN AND W. E, *Contact line dynamics on heterogeneous surfaces*, Phys. Fluids, 23 (2011), 072103.
- [29] W. REN, P. H. TRINH, AND W. E, *On the distinguished limits of the Navier slip model of the moving contact line problem*, J. Fluid Mech., 772 (2015), pp. 107–126.
- [30] M. REYSSAT AND D. QUÉRÉ, *Contact angle hysteresis generated by strong dilute defects*, J. Phys. Chem. B, 113 (2009), pp. 3906–3909.
- [31] J. SNOEIJER AND B. ANDREOTTI, *Moving contact lines: Scales, regimes, and dynamical transitions*, in Annual Reviews of Fluid Mechanics, Annu. Rev. Fluid Mech. 45, Annual Reviews, Palo Alto, CA, 2013.
- [32] A. TURCO, F. ALOUGES, AND A. DESIMONE, *Wetting on rough surfaces and contact angle hysteresis: Numerical experiments based on a phase field model*, ESAIM Math. Model. Numer. Anal., 43 (2009), pp. 1027–1044.
- [33] X.-P. WANG, T. QIAN, AND P. SHENG, *Moving contact line on chemically patterned surfaces*, J. Fluid Mech., 605 (2008), pp. 59–78.
- [34] X.-P. WANG AND X. XU, *A dynamic theory for contact angle hysteresis on chemically rough boundary*, Discrete Contin. Dyn. Syst., 37 (2017), pp. 1061–1073.
- [35] G. WHYMAN, E. BORMASHENKO, AND T. STEIN, *The rigorous derivation of Young, Cassie-Baxter and Wenzel equations and the analysis of the contact angle hysteresis phenomenon*, Chem. Phys. Lett., 450 (2008), pp. 355–359.
- [36] X. XU, *Modified Wenzel and Cassie equations for wetting on rough surfaces*, SIAM J. Appl. Math., 76 (2016), pp. 2353–2374, <https://doi.org/10.1137/15M1038451>.
- [37] X. XU, Y. DI, AND M. DOI, *Variational method for contact line problems in sliding liquids*, Phys. Fluids, 28 (2016), 087101.
- [38] X. XU, Y. DI, AND H. YU, *Sharp-interface limits of a phase-field model with a generalized Navier slip boundary condition for moving contact lines*, J. Fluid Mech., 849 (2018), pp. 805–833.
- [39] X. XU AND X. WANG, *Analysis of wetting and contact angle hysteresis on chemically patterned surfaces*, SIAM J. Appl. Math., 71 (2011), pp. 1753–1779, <https://doi.org/10.1137/110829593>.
- [40] X. XU AND X.-P. WANG, *The modified Cassie’s equation and contact angle hysteresis*, Colloid Polym. Sci., 291 (2013), pp. 299–306.
- [41] X. XU AND X.-P. WANG, *Non-Darcy behavior in two-phase channel flow*, Phys. Rev. E (3), 90 (2014), 023010.